Materials Research. 2023; 26(suppl. 1):e20220566
DOI: https://doi.org/10.1590/1980-5373-MR-2022-0566

Development of Thin Films Formed by Ti-Zr Alloys at Different Frequencies by the HiPIMS Technique

C. J. R. Lustosa[a]*, *J. Stryhalski*[b], *R. L. P. Gonçalves*[a], *E. Bonturim*[a], *O. Florêncio*[c], *M. Massi*[a]

[a]*Universidade Presbiteriana Mackenzie, Escola de Engenharia, 01302-907, São Paulo, SP, Brasil.*
[b]*Instituto Federal de Santa Catarina, 89254-430, Jaraguá do Sul, SC, Brasil.*
[c]*Universidade Federal de São Carlos, 18052-780, Sorocaba, SP, Brasil.*

Received: December 15, 2022; Revised: April 29, 2023; Accepted: June 07, 2023

In this work, thin films based on the Ti-Zr system were studied, deposited on a silicon substrate by the magnetron sputtering technique using simultaneously a combination of High-Power Impulse Magnetron Sputtering (HiPIMS) and Direct Current Magnetron Sputtering (DCMS) sources. The objective of this work is analyzing the effect of varying HiPIMS frequency (300 Hz, 400 Hz, 500 Hz, and 600 Hz) on the characteristics and properties of the thin films. The thickness increased between 300 Hz and 500 Hz, where the thickness measured 563 nm and 732 nm, respectively; then it decreased to 709 nm at 600 Hz. Hardness and elastic moduli also tended to decrease with increasing frequency, and the results for the first property were between 7 GPa and 10.3 Gpa, while the elastic moduli were from 114 Gpa to 157 Gpa, in which lower values were reached at higher frequencies. In the wettability test, lower contact angles were observed for samples with lower frequencies due to their high surface energy, providing better hydrophilic properties.

Keywords: *Ti-Zr alloy, thin film, HiPIMS, biomaterial.*

1. Introduction

Biomaterials are widely used to replace parts of the body or help with the healing process. Rejection, inflammation, and other complications of these materials in the organism must be avoided[1-4]. Ti-Zr alloys have emerged as an interesting alternative biomaterial. The properties of titanium, including high resistance to corrosion, low density, and biocompatibility, are very appreciated and desired[5-7]. Zirconium also has excellent resistance against corrosion and acceptable biocompatibility[8-10].

Many elements can damage health after they corrode and release dangerous ions, including the Ti-6Al-4V alloy, which is one of the alloys most often applied as biomaterials. It contains aluminum, which is associated with neuron disease[11], and vanadium may be responsible for allergic reactions in some organisms[12]. Both titanium and zirconium have no adverse effect on the living organism, as reported in several works[13-15]. These elements combined showed no undesirable response[16], and some results have indicated an improvement in the biocompatibility of the Ti-Zr alloy compared to cp-Ti (Commercially Pure titanium)[17]. When these elements are mixed, this system also has other advantages that improve mechanical properties including increased tensile strength and greater elastic recovery. The tensile strength is superior to commercially pure titanium, making this alloy an alternative for dental and orthopedic applications[18].

In addition, the thin films constituted by Ti-Zr are not toxic, can tolerate cellular growth, and do not impair cellular growth[19]. This alloy can reach high elastic modulus when produced by magnetron sputtering[20] and may even present hydrophobic properties when combined with aluminum[21]. However, few studies have been conducted about thin films deposited by magnetron sputtering for the Ti-Zr system, and as the High-Power Impulse Magnetron Sputtering (HiPIMS) technique is still relatively recent, there is a lack of data in the literature. Therefore, the aim of this paper is to improve the understanding on the behavior of co-sputtering Ti and Zr in DC and HiPIMS sources respectively in different frequencies, furthermore, an assessment was made of the morphological outcomes of the resultant films.

2. Material and Method

The thin films were deposited on polished silicon wafer (100) through magnetron sputtering technique with a combination of DCMS (DC Power Supply 1000 W, ALD) and HiPIMS (HiPIMS Power Supply HIPSTER 1, Lonautics) sources working simultaneously. Targets with a diameter of 2 inches were used, one made of titanium (99.99% pure) on the DCMS and the other of zirconium (99.9% pure) on the HiPIMS source. The depositions were made using argon gas (99.999% pure) with a flow rate of 60 sccm, working pressure of 7.5×10^{-3} Torr for 60 min, with substrate heated at 200 °C, 150 mm distance from the target to the substrate, and bias at -40 VDC. In both sources, 150 W of power was applied. The pulse width of 50 μs was set in the HiPIMS, while the frequency was changed for each deposition, which

*e-mail: cicerojunior15@hotmail.com

provided different duty cycles in HiPIMS, and these values are presented in Table 1. For the depositions, the silicon substrate was cut into pieces with approximate sizes of 10 mm × 15 mm, in which the analyzed film covered an area of 10 mm × 10 mm.

The structural characterization of the samples was done with an X-ray Diffractometer (XRD) Rigaku Miniflex II, with radiation of Cu Kα (λ = 0.154 nm). Using the data obtained from diffractograms, the size of crystallites (D) and microstrains (ε) were calculated using the Williamson-Hall method, represented by Equation 1, where λ is the wave width from diffractometer. The constant k = 0.94 was adopted due to the use of FWHM (Full Width at Half Maximum) in the calculation[22]. β represents the FWHM, θ is the Bragg angle, and these values were obtained by the Origin software, where the calculations were made by the slope intercept equation with βcosθ on the y axis and 4senθ on the x axis.

$$\frac{\beta \cos\theta}{\lambda} = \frac{k}{D} + \frac{4\varepsilon}{\lambda} sen\,\theta \quad (1)$$

The morphology study was carried out using a Scanning Electron Microscope (SEM) (Jeol JSM-6510), and the distribution of the elements on the surface analyzed by the EDS (Energy Dispersive X-Ray Spectroscopy) coupled with the SEM. The thickness of the film was obtained by the profilometer KLA Tencor, T7 model.

The mechanical properties were studied using the nanoindenter Hit 300 from Anton Paar, with a charge of 2 mN, a distance of 30 μm between indentations, and Poisson's ratio of 0.34. The hardness and elastic modulus were measured, while the deformation energies (elastic, plastic, and total) were calculated integrating the curves obtained from the samples. In addition, a wettability test was made on the surface of the thin films to study their surface energy and contact angle using a Kruss Contact Angle Analyzer, model DSA 100B by sessile drop method. For the wettability, water and ethylene glycol were used, the test was performed for 30 seconds. The surface energy was calculated using the values of liquid-vapor interface (γ_{LV}), $\gamma_{LV}{}^{d}$ = 21.8 N.m-1 and $\gamma_{LV}{}^{p}$ = 51.0 N.m-1 for water. Furthermore, $\gamma_{LV}{}^{d}$ = 29.0 N.m-1 and $\gamma_{LV}{}^{p}$ = 19.0 N.m-1 have been attributed to ethylene glycol[23].

3. Results and Discussion

The XRD results in Figure 1 indicate some crystalline structures corresponding to Ti-Zr alloy. The two peaks that appeared in all the samples represent the planar orientation (002) and (200), in which the first is the preferential orientation, widely documented in the literature about this kind of alloy[19,20]. Only the sample deposited at 600 Hz presented one additional peak (100) with considerable intensity, and all peaks correspond to α phase of the Ti-Zr alloy. The Williamson-Hall equation was employed to estimate the crystallite sizes and microstrains, resulting in the values presented in Figure 1. The larger size was found from the lower frequency, at 300 Hz with approximately 246 nm, and the same sample had the greater microstrain of all the thin films deposited. The dimensions of the other crystallites tend to decrease as the frequency increases up to 500 Hz, and the microstrain also decreases. As high temperatures are known to aid diffusion of atoms during thin film growth which increases grain size[24], the heating of the substrate plus the collisions of energetic atoms sputtering at low frequencies[25] could have provided more thermal energy to form larger grains. The energy supplied to the atoms decreases as the frequency increases according to peak current values and the thickness increased, which might explain the low crystallite sizes and microstrain. However, when produced at a higher frequency (600 Hz), the crystallites grew more than in the sample deposited at 400 Hz. However, the microstrain did not surpass the result of the 400 Hz sample, which may be associated with lesser thickness and different chemical compositions that could collaborate with the heat transfer in this sample.

The thin film thickness of all samples was measured by profilometry, as summarized in Table 2. The thickness increased with increasing frequency between 300 Hz to 500 Hz but decreased with 600 Hz. The lesser thickness may be related to the low duty cycle in the depositions, which is smaller with low frequency, causing higher peak current, and as a consequence, the collisions of ions can rise with more energy[25]. An explanation for the greater thickness at 500 Hz could be that at 500 Hz more of the atoms ejected from the target have sufficient energy to reach the substrate without pulling out others already deposited, suffering reflection, or becoming lost along the way.

It is known that high energy particles ejected from the target can reach the substrate and are reflected or desorbed, and the control of this behavior can increase the rate of deposition[26]. At 300 Hz, the peak current measured was 25 A, the other values were 18 A, 11.4 A, and 9.8 A for 400 Hz, 500 Hz, and 600 Hz, respectively. Thus, lower peak currents were obtained at higher frequencies, as reported in the literature[27]. The other possible explanation for the sample at 600 Hz being less thick than the sample at 500 Hz is also related to the energies of the ions that bombard the targets. This could have changed the number of ionized atoms leaving the target, which may have changed the growth rate of the thin film. For Kubart

Table 1. Variable parameters in the HiPIMS: chosen frequency, calculated duty cycle, and measured Peak Current.

Sample	Frequency (Hz)	Duty cycle (%)	Peak Current (A)
N° 1	300	1.5	25
N° 2	400	2	18
N° 3	500	2.5	11.4
N° 4	600	3	9.8

Table 2. Thickness of deposited thin films at their respective HiPIMS deposition frequencies.

Sample	HiPIMS Frequency (Hz)	Thin film thickness (nm)
N° 1	300	563 ± 13
N° 2	400	670 ± 10
N° 3	500	732 ± 6
N° 4	600	709 ± 8

and Aijaz[28], this may be a consequence of gas rarefaction next to the target, because the change in pulse width could heat the gas in front of the target, but the exact mechanism is not well known[28]. The sputter yield in HiPIMS processes for oxides and metals is complex as it involves numerous factors such as type of ions, electron density, composition of neutral and ionized atoms self-sputtering, and working gas recycling as discussed in the literature[29,30].

SEM micrographs of the samples in Figure 2 illustrate different amounts of porosity and white microparticles on the surface, which were influenced by their parameters of deposition. The sample deposited at 300 Hz was the alloy with the greatest porosity, while in the samples at 400 Hz and 500 Hz, this type of defect was not found but returned in smaller quantities than the sample at 300 Hz on the surface of the sample produced at 600 Hz. Studies with EDS on the microparticles observed a great amount of titanium in their constitution. Other works found the same particles when the alloy had titanium as the main element of the alloy[31,32], and the formation of these structures may occur when the atoms are going toward the substrate, forming clusters that settle on the film surface[33]. The deposition of zirconium was higher at 500 Hz, decreasing at other frequencies. The possible explanation may be related to the phenomena

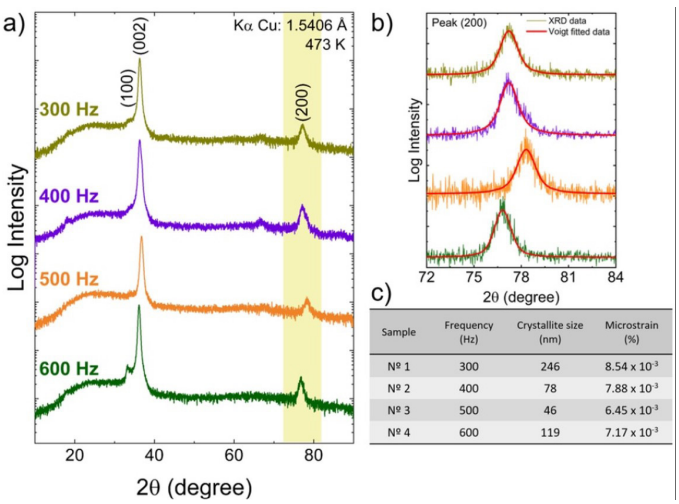

Sample	Frequency (Hz)	Crystallite size (nm)	Microstrain (%)
Nº 1	300	246	8.54×10^{-3}
Nº 2	400	78	7.88×10^{-3}
Nº 3	500	46	6.45×10^{-3}
Nº 4	600	119	7.17×10^{-3}

Figure 1. XRD patterns of the thin film samples grown at 300, 400, 500, and 600 Hz, the Voigt fitting curves of peak (200), and their respective crystallite sizes calculated by Williamson-Hall equation.

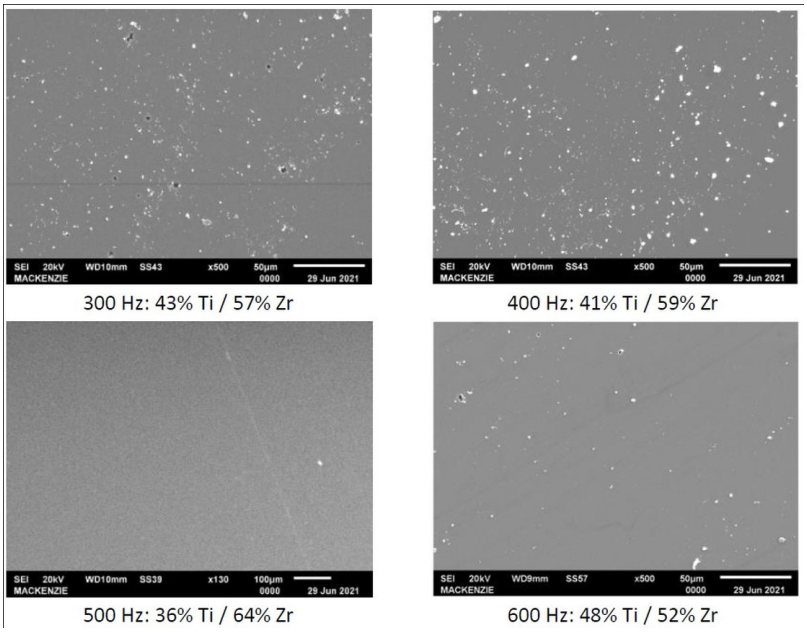

Figure 2. SEM micrographs of the thin films deposited on silicon.

described above, which are associated with atoms that had different energies and changed the number of ionized Zr atoms from HiPIMS leaving the target, changing the growth rate of both elements during co-sputtering as discussed in previous works[34,35].

The hardness measurements showed a behavior inversely proportional to the frequency up to 500 Hz, as can be seen in Figure 3a. At 600 Hz, the hardness grew to almost the same as at 400 Hz. The high peak current possibly influenced the increase in the hardness of the deposited thin films, as was observed in a previous work[36]. Greater stress occurred in thin films that were deposited at low frequencies[35], and this may explain the hardness values. The high bombardment of ions with higher energy in the targets, releasing more energetic atoms toward the substrate, could have influenced the microstrain shown in Figure 1. A large strain gradient greatly influences the resistance to plastic deformation when the scale decreases[37], which may have influenced the hardness of the thin films studied.

The elastic moduli result in Figure 3b showed that the samples with lower frequencies had higher values. This property is very important for applications in the biomedical field, because alloys with high elastic modulus normally avoid the transmission of tension to bones, which can lead to stress shielding. The sample deposited at 600 Hz has approximately 115 GPa, which is very close to pure titanium[38] and Ti-6Al-4V[39], alloys widely used in prothesis composition. The samples deposited at 500 Hz and 400 Hz presented 136 GPa and 157 GPa, respectively, and their standard deviation points to many heterogeneous regions with atomic bonds of different strengths[40,41]. Even with elastic modulus very high, these values are inferior to stainless steel, cobalt alloys, and Co-Cr alloys, also used as biomaterials[42,43].

The total deformation energy was also calculated with the results from indentations, specifically using the curves in Figure 3c. The values of total deformation were 6.02×10^7 N.m, 6.50×10^7 N.m, 7.53×10^7 N.m, and 7.24×10^7 N.m from 300 Hz, 400 Hz, 500 Hz, and 600 Hz, respectively. When the plastic or elastic deformations were analyzed and calculated, more elastic deformations were observed in the sample deposited at 300 Hz and at 600 Hz, with 51% and 45%, respectively. The plastic deformation was greater in the samples deposited at 500 Hz and 400 Hz, with amounts of 59% and 57%, respectively.

Wettability tests were used to study the surface energy of the samples and the contact angle formed, correlating to deposition frequencies. Figure 4 illustrates the correlation between the contact angle and the frequencies because the values increased as the other rose. The sample deposited at 300 Hz had a contact angle of 35.7°, while the other angles were 51.9°, 52.2°, and 64.8° for 400 Hz, 500 Hz, and 600 Hz, respectively. This means that decreasing frequency produced more hydrophilic surfaces, which could allow the adhesion of polar organic matter such as cells, and even might improve the osseointegration process. The variations of the contact angles were possible because the samples have different surface energies, and surface atoms have more energy than atoms surrounded by others within the sample, thus the surface atoms interact with other external atoms.

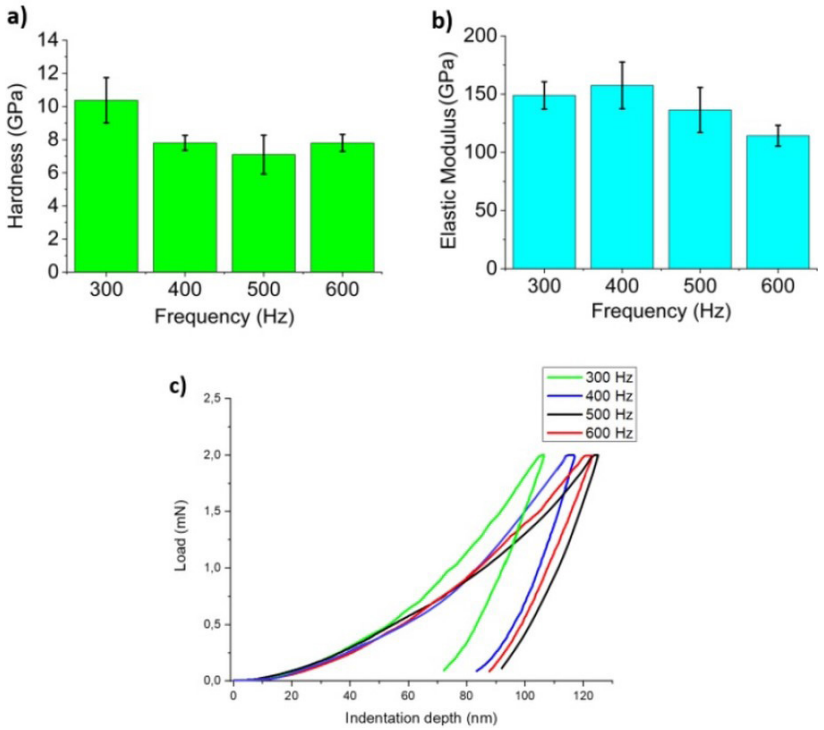

Figure 3. Results from nanoindentation for a) Hardness, b) Elastic Moduli, and c) average curves of the thin films grown at different frequencies.

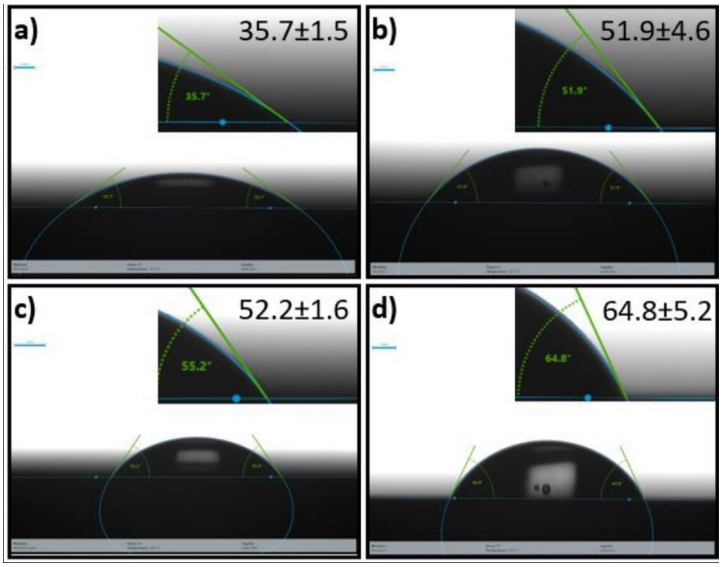

Figure 4. Contact angles obtained in the wettability test for thin films grown at a) 300 Hz, b) 400 Hz, c) 500 Hz, and d) 600 Hz.

4. Conclusion

The thin film characterization showed the effects of the frequency on the properties and morphology of the samples. First, in the profilometry results, the samples deposited with lower frequencies were less thick, probably due to the high energy imparted to the removed atoms by highly energized ions. Despite the lesser thickness, the samples deposited at low frequencies reached higher hardness properties that can help to mitigate wear.

Another interesting result came from the wettability test, which found the connection between frequency and contact angle, showing a directly proportional behavior in this work. The samples formed at low frequencies presented the lower contact angle, and the wettability decreased as the frequency increased. It is widely reported in the literature that the Ti-Zr system has no toxic effect on living organisms; thus, these films could not only protect against the release of dangerous ions but also improve the osseointegration due to their excellent wettability[44,45].

5. Acknowledgments

The authors would like to thank Instituto Presbiteriano Mackenzie, Anton Paar, and MackPesquisa for the financial and technical support in this work. We also thank the financial support of CAPES (grant number 88881.310340/2018-01).

6. References

1. Elias CN, Lima JHC, Valiev R, Meyers MA. Biomedical applications of titanium and its alloys. JOM. 2008;60(3):46-9. http://dx.doi.org/10.1007/s11837-008-0031-1.
2. Antoniac IV, editor. Handbook of bioceramics and biocomposites. Cham: Springer; 2016.
3. Preetha B, Sreekala MS, Sabu T. Fundamental biomaterials: metals. Duxford: Woodhead Publishing; 2018.
4. Geetha M, Singh AK, Asokamani R, Gogia AK. Ti based biomaterials, the ultimate choice for orthopaedic implants – a review. Prog Mater Sci. 2009;54:397-425. http://dx.doi.org/10.1016/j.pmatsci.2008.06.004.
5. Long M, Rack HJ. Titanium alloys in total joint replacement: a materials science perspective. Biomaterials. 1998;19(18):1621-39. http://dx.doi.org/10.1016/S0142-9612(97)00146-4.
6. Rack HJ, Qazi JI. Titanium alloys for biomedical applications. Mater Sci Eng C. 2006;26(8):1269-77. https://doi.org/10.1016/j.msec.2005.08.032.
7. Niinomi M. Recent research and development in titanium alloys for biomedical applications and healthcare goods. Sci Technol Adv Mater. 2003;4(5):445-54. http://dx.doi.org/10.1016/j.stam.2003.09.002.
8. Chen L, Li J, Zhang Y, Lu W, Zhang L, Wang L et al. Effect of low-temperature pre-deformation on precipitation behavior and microstructure of a Zr-Sn-Nb-Fe-Cu-O alloy during fabrication. J Nucl Sci Technol. 2016;53(4):496-507. http://dx.doi.org/10.1080/00223131.2015.1059776.
9. Zinkle SJ, Was GS. Materials challenges in nuclear energy. Acta Mater. 2013;61(3):735-58. http://dx.doi.org/10.1016/j.actamat.2012.11.004.
10. Pratama NR, Faizal F, Prajitno DH. Corrosion behavior of ternary Zr-25Ti-5Sn alloy doped with Ge as biomaterials implant in simulation body fluid solution. Int J Mech Eng Technol Appl. 2020;1(2):59-67. http://dx.doi.org/10.21776/MECHTA.2020.001.02.4.
11. Walker PR, Leblanc J, Sikorska M. Effects of aluminum and other cations on the structure of brain and liver chromatin. Biochemistry. 1989;28(9):3911-5. http://dx.doi.org/10.1021/bi00435a043.
12. Engelhart S, Segal RJ. Allergic reaction to vanadium causes a diffuse eczematous eruption and titanium alloy orthopedic implant failure. Cutis. 2017;99(4):245-9.
13. Deng L, Wang S, Wang P, Kühn U, Pauly S. Selective laser melting of Ti-based bulk metallic glass. Mater Lett. 2018;212(1):346-9. http://dx.doi.org/10.1016/j.matlet.2017.10.130.
14. Duygulu O, Kaya AA, Oktay G, Sahin FC. Diffusion bonding of magnesium, zirconium and titanium as implant material. Mater Sci Forum. 2017;546-549:417-20. http://dx.doi.org/10.4028/www.scientific.net/MSF.546-549.417.
15. Samuel S, Nag S, Nasrazadani S, Ukirde V, El Bouanani M, Mohandas A et al. Corrosion resistance and in vitro response of laser-deposited Ti-Nb-Zr-Ta alloys for orthopedic applications.

J Biomed Mater Res A. 2010;94(4):1251-6. http://dx.doi.org/10.1002/jbm.a.32782.
16. Gómez-Florit M, Xing R, Ramis JM, Taxt-Lamolle S, Haugen HJ, Lyngstadaas SP et al. Human gingival fibroblasts function is stimulated on machined hydrided titanium zirconium dental implants. J Periodontal Res. 2014;42:30-8. http://dx.doi.org/10.1111/jre.12121.
17. Ikarashi Y, Toyoda K, Kobayashi E, Doi H, Yoneyama T, Hamanaka H et al. Improved biocompatibility of titanium-zirconium (Ti-Zr) alloy: tissue reaction and sensitization to Ti-Zr alloy compared with pure Ti-Zr in rat implantation study. Mater Trans. 2005;46(10):2260-7. http://dx.doi.org/10.2320/matertrans.46.2260.
18. Ho WF, Chen WK, Wu SC, Hsu HC. Structure, mechanical properties, and grindability of dental Ti–Zr alloys. J Mater Sci Mater Med. 2008;19(10):3179-86. http://dx.doi.org/10.1007/s10856-008-3454-x.
19. Tondela JPS. Filmes finos de titânio-zircónio nanoestruturados para osteointegração [thesis]. Coimbra: Universidade de Coimbra; 2014.
20. Rodríguez-Hernández MG, Jiménez O, Alvarado-Hernández F, Flores M, Andrade E, Canto CE et al. The effect of C content on the mechanical properties of Ti-Zr coatings. J Mech Behav Biomed Mater. 2015;49:269-76. http://dx.doi.org/10.1016/j.jmbbm.2015.05.004.
21. Tang JF, Huang PY, Lin JH, Liu TW, Yang FC, Chang CL. Microstructure and antimicrobial properties of Zr-Cu-Ti thin-film metallic glass deposited using high-power impulse magnetron sputtering. Materials. 2022;15:2461. http://dx.doi.org/10.3390/ma15072461.
22. Warren BE. X-ray diffraction. New York: Dover Publications; 1990.
23. Kozbial A, Li Z, Conaway R, Mcginley R, Dhingra S, Vahdat V et al. Study on the surface energy of graphene by contact angle measurements. Langmuir. 2014;30:8598-606. http://dx.doi.org/10.1021/la5018328.
24. Gudmundsson JT, Anders A, Keudell A. Foundations of physical vapor deposition with plasma assistance. Plasma Sources Sci Technol. 2022;31(8):083001. http://dx.doi.org/10.1088/1361-6595/ac7f53.
25. Chang CL, Shih SG, Chen PH, Chen WC, Ho CT, Wu WY. Effect of duty cycles on the deposition and characteristics of high power impulse magnetron sputtering TiN thin films. Surf Coat Tech. 2014;259(25):232-7. http://dx.doi.org/10.1016/j.surfcoat.2014.03.011.
26. Bobzin K, Brögelmann T, Brugnara RH. Aluminum-rich HPPMS (Cr1–xAlx)N coatings deposited with different target compositions and at various pulse lengths. Vacuum. 2015;122:201-7. http://dx.doi.org/10.1016/j.vacuum.2015.09.028.
27. Severin S, Naveed M, Weiss S. Effect of HPPMS pulse-frequency on plasma discharge and deposited AlTiN coating properties. Adv Mater Sci Eng. 2017;2017:1-18. http://dx.doi.org/10.1155/2017/4850908.
28. Kubart T, Aijaz A. Evolution of sputtering target surface composition in reactive high power impulse magnetron sputtering. J Appl Phys. 2017;121(17):171903. http://dx.doi.org/10.1063/1.4977814.
29. Gudmundsson J, Lundin D, Brenning N, Raadu M, Huo C, Minea T. An ionization region model of the reactive Ar/O_2 high power impulse magnetron sputtering discharge. Plasma Sources Sci Technol. 2016;25(6):065004. http://dx.doi.org/10.1088/0963-0252/25/6/065004.
30. Depla D, Heirwegh S, Mahieu S, Haemers J, Gryse R. Understanding the discharge voltage behavior during reactive sputtering of oxides. J Appl Phys. 2007;101(1):013301. http://dx.doi.org/10.1063/1.2404583.
31. Constantin DG, Moura C, Munteanu D, Cunha L. The influence of oxygen flow during deposition on the structural, mechanical and tribological properties of titanium oxide magnetron sputtered thin films. J Optoelectron Adv Mater. 2012;14(10):964-70.
32. Ivanova AA, Surmeneva MA, Shugurov VV, Kovak NN, Shulepov IA, Surmenev RA. Physico-mechanical properties of Ti-Zr coatings fabricated via ion-assisted arc-plasma deposition. Vacuum. 2018;149:129-33. http://dx.doi.org/10.1016/j.vacuum.2017.12.024.
33. Oliver WC, Pharr GM. An improved technique for determining hardness and elastic modulus using load and displacement sensing indentation experiments. J Mater Res. 1992;7:1564-83. http://dx.doi.org/10.1557/JMR.1992.1564.
34. Nedfors N, Mockuté A, Palisaitis J, Persson POA, Näslund L, Rosén J. Influence of pulse frequency and bias on microstructure and mechanical properties of TiB_2 coatings deposited by high power impulse magnetron sputtering. Surf Coat Tech. 2016;304:203-10. http://dx.doi.org/10.1016/j.surfcoat.2016.06.086.
35. Mei HJ, Ding JC, Xiao XL, Luo QS, Wang R, Zhang Q et al. Influence of pulse frequency on microstructure and mechanical properties of Al-Ti-V-Cu-N coatings deposited by HIPIMS. Surf Coat Tech. 2021;405:126514. http://dx.doi.org/10.1016/j.surfcoat.2020.126514.
36. Bagcivan N, Bobzin K, Grundmeier G, Wiesing M, Ozcan O, Kunze C et al. Influence of HPPMS pulse length and inert gas mixture on the properties of (Cr,Al)N coatings. Thin Solid Films. 2013;549:192-8. http://dx.doi.org/10.1016/j.tsf.2013.06.036.
37. Fleck NA, Muller GM, Ashby MF, Hutchinson JW. Strain gradient plasticity: teory and experiment. Acta Metall Mater. 1994;42(2):475-87. http://dx.doi.org/10.1016/0956-7151(94)90502-9.
38. Disegi J. Implant mater. Unalloyed titanium. 6th ed. West Chester: Synthes; 2008.</bok> p. 1-18
39. Long M, Rack HJ. Titanium alloys in total joint replacement: a materials science perspective. Biomaterials. 1998;19(18):1621-39. http://dx.doi.org/10.1016/S0142-9612(97)00146-4.
40. Lin BB, Auernhammer J, Schäfer J, Meckel T, Stark R, Biesalski M et al. Humidity influence on mechanics of paper materials: joint numerical and experimental study on fiber and fiber network scale. Cellulose. 2022;29:1129-48. http://dx.doi.org/10.1007/s10570-021-04355-y.
41. Padmavathi DA. Potential energy curves & material properties. Mater Sci Appl. 2011;2(2):97-104. http://dx.doi.org/10.4236/msa.2011.22013.
42. Park J, Lakes RS. Biomaterials: an introduction. New York: Springer; 2007.
43. Davies JR. Handbook of materials for medical devices. Materials Park: ASM International; 2003.
44. Ou PH, Zhang TM, Wang JY, Li C, Shao CS, Ruan JM. Bone response in vivo of Ti-45Zr alloy as dental implant material. J Mater Sci Mater Med. 2022;33(47):1-12. http://dx.doi.org/10.1007/s10856-022-06664-5.
45. Cordeiro JM, Faverani LP, Grandini CR, Rangel EC, Cruz NC, Nociti FH Jr et al. Characterization of chemically treated Ti-Zr system alloys for dental implant application. Mater Sci Eng C. 2018;92:849-61. http://dx.doi.org/10.1016/j.msec.2018.07.046.